H. 知的財産権の出願・登録状況（予定も含む）

1. 特許取得　　：なし
2. 実用新案登録：なし
3. その他　　：なし

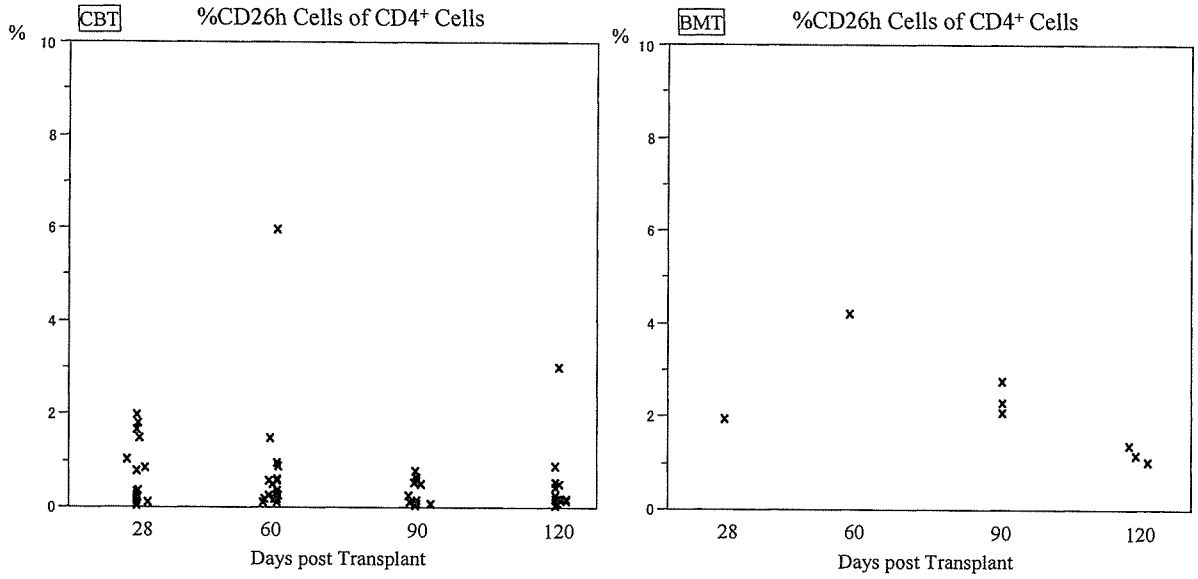

Ⅲ.　研究成果の刊行に関する一覧表

＜研究成果の刊行に関する一覧表＞

【雑　誌】

発表者氏名	論文タイトル名	発表誌名	巻号	ページ	出版年
Ohnuma K, Uchiyama M, Yamochi T, Nishibashi K, Hosono O, Takahashi N, Kina S, Tanaka H, Lin X, Dang NH, Morimoto C	Caveolin-1 triggers T-cell activation via CD26 in association with CARMA1.	J Biol Chem., in press (2007)			
Thompson MA, Ohnuma K, Abe M, Morimoto C, Dang NH	CD26/Dipeptidyl Peptidase IV as a Novel Therapeutic Target for Cancer and Immune Disorders.	Mini-Reviews in Medicinal Chemistry	7	253-273	2007
Ohnuma-Ishikawa K, Morio T, Yamada T, Sugawara Y, Ono M, Nagasawa M, Yasuda A, Morimoto C, Ohnuma K, Dang NH, Hosoi H, Verdin E, Mizutani S	Knockdown of XAB2 enhances all-trans retinoic acid-induced cellular differentiation in all-trans retinoic acid-sensitive and -resistant cancer cells.	Cancer Res	67	1019-1029	2007
Inamoto S, Iwata S, Inamoto T, Nomura S, Sasaki T, Urasaki Y, Hosono O, Kawasaki H, Tanaka H, Dang NH, Morimoto C	Crk-associated substrate lymphocyte type regulates transforming growth factor-beta signaling by inhibiting Smad6 and Smad7.	Oncogene	26	893-904	2007
Inamoto T, Yamochi T, Ohnuma K, Iwata S, Kina S, Inamoto S, Tachibana M, Katsuoka Y, Dang NH, Morimoto C	Anti-CD26 monoclonal antibody-mediated G1-S arrest of human renal clear cell carcinoma Caki-2 is associated with retinoblastoma substrate dephosphorylation, cyclin-dependent kinase 2 reduction, p27(kip1) enhancement, and disruption of binding to the extracellular matrix.	Clin Cancer Res	12	3470-3477	2006
Ohnuma K, Inoue H, Uchiyama M, Yamochi T, Hosono O, Dang NH, Morimoto C	T-cell activation via CD26 and caveolin-1 in rheumatoid synovium.	Mod Rheumatol	16	3-13	2006

発表者氏名	論文タイトル名	発表誌名	巻号	ページ	出版年
船越信介、岩男 泰、芳沢茂雄、久松理一、岡本 晋、高石官均、井上 詠、今枝博之、緒方晴彦、杉野吉則、向井万起男、日比紀文	自然軽快したcap polyposisの1例	Progress of Digestive Endoscopy	68	140-141	2006
志賀洋史、船越信介、首村智久、高山哲朗、芹澤 宏、渡辺憲明、常松 令、金子文彦、熊谷直樹、森永正二郎、 土本寛二、岩男泰、日比紀文	大腸全摘術後の回腸嚢炎・多発関節炎に白血球除去両方が奏功した潰瘍性大腸炎の1例	Progress of Digestive Endoscopy	69	100-101	2006
Mosohoshi Y, Matsuoka K, Chinen H, Kamada N, Sato T, Hisamatsu T, Okamoto S, Inoue N, Takaishi H, Ogata H, Iwao Y, and Hibi T	Inhibition of neutrophil elastase prevents the development of murine dextran sulfate sodium-induced colitis.	J Gastroenterol	41	318-324	2006
Hibi T and Ogata H	Novel pathophysiological concepts of inflammatory bowel disease.	J Gastroenterol	41	10-16	2006
Hisamatsu T, Inoue N, Yajima T, IzumiyaM, IchikawaH, and Hibi T	Psychological aspects of inflammatory bowel disease.	J Gastroenterol	42	34-40	2007
Uesato N, Fukui K, Maruhashi J, Tajima N, Tojo A, Watanabe Y	JTE-607, a multiple cytokine production inhibitor, ameliorates disease in a SCID mouse xenograft acute myeloid leukemia model.	Exp Hematol.	34	1385-1392	2006
Tomonari A, Takahashi S, Ooi J, Nakaoka T, Takasugi K, Uchiyama M, Tsukada N, Konuma T, Iseki T, Tojo A, Asano S	Cord blood transplantation for acute myelogenous leukemia using a conditioning regimen consisting of granulocyte colony-stimulating factor-combined high-dose cytarabine, fludarabine, and total body irradiation.	European Journal of Haematology	77	46-50	2006

発表者氏名	論文タイトル名	発表誌名	巻号	ページ	出版年
Inoue Y, Tojo A, Sekine R, Soda Y, Kobayashi S, Nomura A, Izawa K, Kitamura T, Okubo T, Ohtomo K	In vitro validation of bioluminescent monitoring of disease progression and therapeutic response in leukaemia model animals.	European Journal of Nuclear Medicine and Molecular Imaging	33	557-65	2006
Konuma T, Tomonari A, Takahashi S, Ooi J, Tsukada N, Yamada T, Sato H, Nagayama H, Iseki T, Tojo A, Asano S	Early-onset thyrotoxicosis after unrelated cord blood transplantation for acute myelogenous leukemia.	International Journal of Hematology	83	348-50	2006
Inoue Y, Izawa K, Tojo A, Sekine R, Okubo T, Ohtomo K	Light emission requires exposure to the atmosphere in ex vivo bioluminescence imaging.	Molecular Imaging	5	53-6	2006
Koide N, Yamada T, Shibata R, Mori T, Fukuma M, Yamazaki K, Aiura K, Shimazu M, Hirohashi S, Nimura Y, Sakamoto M	Establishment of Perineural Invasion Models and Analysis of Gene Expression Revealed an Invariant Chain (CD74) as a Possible Molecule involved in Perineural Invasion in Pancreatic Cancer	Clin Cancer Reseach	12	2419-2426	2006
Ohteki T, Tada H, Ishida K, Sato T, Maki C, Yamada T, Hamuro J, Koyasu S	Essential roles of DC-derived IL-15 as a mediator of inflammatory responses in vivo.	J Exp Med	203	2329-2338	2006
Kawasaki H, Tsunoda K, Hata T, Ishii K, Yamada T, Amagai M	Synergistic pathogenic effects of combined mouse monoclonal anti-desmoglein 3 IgG antibodies on pemphigus vulgaris blister formation.	J Invest Dermatol.	126	2621-2630	2006
Kiuchi S, Yamada T, Kiyokawa N,Saito T,Fujimoto J, Yasue H	Genomic structure of swine taste receptor family 1 member 3, TAS1R3, and its expression in tissues	Cytogenetic and Genome Research	115	51-61	2006

発表者氏名	論文タイトル名	発表誌名	巻号	ページ	出版年
Awaya N, Adachi A, Mori T, Kamata H, Nakahara J, Yokoyama K, Yamada T, Kizaki M, Sakamoto M, Ikeda Y, Okamoto S.	Fulminant Epstein-Barr virus (EBV)-associated T-cell lymphoproliferative disorder with hemophagocytosis following autologous peripheral blood stem cell transplantation for relapsed angioimmunoblastic T-cell lymphoma.	Leuk Res	30	1059-62	2006

Ⅳ.　研究成果の別刷

JBC Papers in Press. Published on February 6, 2007 as Manuscript M609157200
The latest version is at http://www.jbc.org/cgi/doi/10.1074/jbc.M609157200

Category: Mechnanisms of Signal Transduction

Caveolin-1 triggers T-cell activation via CD26 in association with CARMA1

Kei Ohnuma *, Masahiko Uchiyama *, Tadanori Yamochi *,

Kunika Nishibashi *, Osamu Hosono *, Nozomu Takahashi*, Shinichiro Kina*,

Hirotoshi Tanaka *, Xin Lin #, Nam H. Dang †, and Chikao Morimoto * ‡

*** Division of Clinical Immunology, Advanced Clinical Research Center, Institute of Medical Science, University of Tokyo, 4-6-1, Shirokanedai, Minato-ku, Tokyo 108-8639, Japan.**

 # Department of Molecular and Cellular Oncology, University of Texas, MD Anderson Cancer Center, Houston, TX 77030, U.S.A.

† Department of Hematologic Malignancies, Nevada Cancer Institute, Las Vegas, NV 89135, U.S.A.

Running Title: Caveolin-1 activates T-cell via CD26

The first and second authors equally contributed to this work.

‡ Address correspondence to Dr. C. Morimoto, Division of Clinical Immunology, Advanced Clinical Research Center, Institute of Medical Science, University of Tokyo, 4-6-1, Shirokanedai, Minato-ku, Tokyo 108-8639, Japan; TEL +81-354-495-546 FAX+81-354-495-448 E-mail: morimoto@ims.u-tokyo.ac.jp

CD26 is a widely distributed 110-kDa cell surface glycoprotein, having an important role in T-cell costimulation. We previously demonstrated that CD26 binds to caveolin-1 in antigen-presenting cells (APC), and that following exogenous CD26 stimulation, Tollip and IRAK-1 disengage from caveolin-1 in APC. IRAK-1 is then subsequently phosphorylated to upregulate CD86 expression, resulting in subsequent T cell proliferation. However, it is unclear whether caveolin-1 is a costimulatory ligand for CD26 in T-cell. Using soluble caveolin-1-Fc fusion protein, we now showed that caveolin-1 is the costimulatory ligand for CD26, and that ligation of CD26 by caveolin-1 induces T-cell proliferation and NF-κB activation in a TCR/CD3-dependent manner. We also demonstrated that the cytoplasmic tail of CD26 interacts with CARMA1 in T-cells, resulting in signaling events that lead to NF-κB activation. Ligation of CD26 by caveolin-1 recruits a complex consisting of CD26, CARMA1, Bcl10, and IKKβ to lipid rafts. Taken together, our findings hence provide novel insights into the regulation of T-cell costimulation via the CD26 molecule.

CD26 is a 110-kDa cell surface glycoprotein with known dipeptidyl peptidase IV (DPPIV, EC3.4.14.5) activity in its extracellular domain (1-3), capable of cleaving amino-terminal dipeptides with either L-proline or L-alanine at the penultimate position (2). CD26 activity is dependent on cell type and the microenvironment, factors that can influence its multiple biological roles (*reviewed in* (4-8)). While CD26 expression is enhanced following activation of resting T-cells, CD4+CD26^{high} T-cells respond maximally to recall antigens such as tetanus

toxoid (9,10). Crosslinking of CD26 and CD3 with solid-phase immobilized monoclonal antibodies (mAbs) can induce T-cell costimulation and IL-2 production by CD26+T-cells (2,7,10). In addition, anti-CD26 antibody treatment of T-cells enhances tyrosine phosphorylation of signaling molecules such as CD3ζ and $p56^{lck}$ (11,12). Moreover, DPPIV activity is required for CD26-mediated T-cell costimulation (13). CD26 may have therefore an important role in T-cell biology and overall immune function. However, the costimulatory ligand of CD26 has not yet been identified, and the proximal signaling events following CD26 engagement in T-cell remain to be determined.

In our previous report, we identified caveolin-1 in antigen-presenting cell (APC) as a binding protein for CD26 and demonstrated that CD26 on activated memory T-cells directly faces caveolin-1 on tetanus toxoid-loaded monocytes in the contact area, which was revealed as the immunological synapse for T-cell-APC interaction (14). Moreover, we showed that residues 201 to 211 of CD26 along with the serine catalytic site at residue 630, which constitute a pocket structure of CD26/DPPIV, contribute to binding to caveolin-1 scaffolding domain (14). More recently, we demonstrated that caveolin-1 binds to Tollip (Toll-interacting protein) and IRAK-1 (interleukin-1 receptor associated serine/threonine kinase 1) in the membrane of tetanus toxoid-loaded monocytes and that following exogenous CD26 stimulation, Tollip and IRAK-1 disengage from caveolin-1, with IRAK-1 being subsequently phosphorylated to upregulate CD86 expression (15). It is conceivable that the interaction of CD26 with caveolin-1 on antigen-loaded monocytes results in CD86 upregulation, therefore enhancing the subsequent interaction of CD86 and CD28 on T-cells to induce antigen-specific T-cell proliferation and activation. However, it is unclear whether caveolin-1 itself is the costimulatory ligand for T-cell CD26.

Recent studies have demonstrated that a newly identified membrane-associated guanylate-kinase-like (MAGUK) molecule, CARMA1, is required for TCR/CD3-CD28 costimulation-induced NF-κB activation and functions downstream of protein kinase C θ (PKCθ) (16-18). CARMA1, which is predominantly expressed in thymus, spleen, and peripheral blood leukocytes, contains an N-terminal caspase-recruitment domain (CARD) followed by a coiled-coil domain (C-C), a PDZ domain, a SH3 domain, and a guanylate kinase (GUK)-like domain (19,20). After TCR/CD3-CD28 costimulation or PMA-CD28 stimulation, CARMA1 is phosphorylated by PKCθ, followed by association with Bcl10 and MALT1, and recruitment of these complexes into lipid rafts (21-23). The recruitment of the CARMA1-Bcl10-MALT1 complex activates IκB kinase (IKK) through an ubiquitin-dependent pathway, leading to activation of NF-κB (24-27). However, it remains to be determined whether CARMA1 is associated with lipid rafts directly or is recruited to lipid rafts via undetermined lipid raft-interacting proteins in the immunological synapse of T-cells.

In the present study, using recombinant immunoglobulin (Ig)-caveolin-1 fusion proteins, we identify caveolin-1 as the costimulatory ligand for CD26, and demonstrate that the N-terminal domain of caveolin-1 induces T-cell proliferation and cytokine production via CD26 costimulation. Furthermore, we show that CARMA1 is bound to the cytoplasmic tail

of dimeric CD26 on T-cells, and that this interaction of CD26 and CARMA1 plays a pivotal role in CD26-mediated T-cell costimulation. Our data hence identify a previously unknown ligand for CD26 as a costimulatory molecule while elucidating the mechanisms involved in CD26-mediated T-cell activation and differentiation.

EXPERIMENTAL PROCEDURES

Expression and Purification of Fc proteins - For initial attempts at expression of soluble forms of Fc-fusion proteins, human IgG_1 Fc cassette vector was made using pCAG-EB6-MCS vector (28,29). The 3' portion of this cassette vector corresponding to human Ig Cγ1 (Fcγ1) sequencing (comprising hinge+CH2+CH3 regions) was made by polymerase-chain reaction (PCR). The all primer information used in this study is described in the Supplementary document. The 5' portion of the cassette vector containing the signal peptide from human E-cadherin (huECDSP) was made by PCR. Final constructs were assembled by ligating both fragments of *Hind* III-Fcγ1-*EcoR*I and *Sal* I-huECDSP-*Hind* III into *Sal I/EcoR* I cleaved pCAG-EB6-MCS (pCAG-EB6-huECDSP-Fcγ1). The N-terminal domain of human caveolin-1 (CavNT) was made by PCR, and constructed into pCAG-EB6-huECDSP-Fcγ1 (pCAG-EB6-huECDSP-CavNT-Fcγ1). With the same methods, the N-terminal domain with deletion of the scaffolding domain (CavNTΔSCD) was made by PCR (pCAG-EB6-huECDSP-CavNTΔSCD-Fcγ1). The Fc fusion protein containing amino acids 1-10 of human CD26 cytoplasmic tail (CD26 AA1-10) was constructed in identical fashion, using the primers described in the Supplementary document (pCAG-EB6-huECDSP-CD26 AA1-10-Fcγ1).

For expression of Fc fusion proteins, FreeStyle™ 293 Expression System was used according to the manufacturer's instruction (Invitrogen). The Fc fusion proteins expressed in the culture supernatant were then purified by affinity chromatography on Protein A-Sepharose (BioRad) followed by size-exclusion purification on Microcon Centrifugal Filter Devices (Millipore), and sterilized using ϕ 0.22μm filter-microcentrifugation tube Spin-X (Corning).

Cells and Reagents - HEK293FT human embryonal kidney, Jurkat T-cell line (JKTwt), and Jurkat T-cells stably transfected with human CD26 (J.CD26wt) were grown as described previously (2,13,14). CARMA1-deficient Jurkat T-cell line, JPM50.6, was developed in the laboratory of Dr. Xin Lin as described elsewhere (18). Human peripheral blood T-cells were purified from peripheral blood mononuclear cells using MACS Pan T-cell Isolation Kit II (Miltenyi), collected from healthy adult volunteers and incubated according to the methods described previously (30). Informed consent was obtained from healthy adult volunteers. Biotinylation of recombinant proteins or antibody was generated using EZ-Link™ Sulfo-NHS-LC-Biotin reagents according to the manufacturer's instruction (PIERCE). Protease inhibitor cocktail, phosphatase inhibitor cocktail, and poly-L-lysin were from Sigma-Aldrich. Water soluble digitonin was purchased from WAKO Pure Chemicals Industries Ltd.

BIAcore™ Analysis of Affinity of Caveolin-1-CD26 interaction - Experiments were carried out on a

BIAcore™ J (Biacore JAPAN) using HBS buffer (25mM HEPES (pH7.4), 150mM NaCl, 3.4mM EDTA, 0.005% surfactant P20) supplied by the manufacturer (Biacore AB). Each of Fcγ1, NT-Fc or NTΔSCD-Fc was coupled in 10mM sodium acetate (pH5.0) to a research grade CM5 sensor chip (Biacore AB) using the Amine Coupling Kit (Biacore AB), with an activating time of 5 minutes, resulting in immobilization of ~5,000-6,000 response units (RU). The surface of the chip was washed with 5mM NaOH after coupling. NaOH (5mM) was used also to regenerate immobilized Fcγ1, NT-Fc or NTΔSCD-Fc chips after each experiment. Recombinant soluble CD26 (rsCD26), comprising the extracellular region of human CD26, was prepared as described previously (30,31). rsCD26 at various concentrations (50nM, 25nM, 12.5nM, 6.3nM, 3.2nM, and 1.6nM) was then injected for 120 seconds over immobilized Fcγ1, NT-Fc or NTΔSCD-Fc chips. Equilibrium binding analysis was performed as described elsewhere (32), using the BIA evaluation software Version 2.1 (BIAcore AB).

Generating Stable Transfectants - The construct of V5-tagged full-length human CD26 (pEF6/V5-CD26wt) was made by PCR, using the primers described in the Supplementary document. The amplified products were cloned into pEF6/V5-His B vector (Invitrogen) at *BamH I/EcoR* I site. The CD26-CD10 chimeric receptor was composed of the N-terminal cytoplasmic region of human CD10 (1-23 amino acid position) ligated to the transmembrane and extracellular regions of human CD26 (7-766 amino acid position), which were made by PCR. The construct of V5-tagged monomeric human CD26 (CD26H750E), which has histidine replacing glutamic acid as a point mutation at amino acid position 750, was made by site-directed mutagenesis method using pEF6/V5-CD26w as a template with the primers described in the Supplementary document. After constructs were confirmed by DNA sequencing, plasmids were transfected to Jurkat T-cells using Nucleofector II device according to the manufacturer's instruction (amaxa biosystems). Two days after transfection of indicated plasmids, the cells were selected for Blasticidin (1μg/ml) resistance for 4 weeks. Single clone cells expressing CD26wt (V5-CD26wt), CD26-CD10 (V5-CD26+CD10 cyto), and CD26H750E were then selected using standard limiting dilution method.

For rescue experiments, the CARMA1-deficient Jurkat cell line JPM50.6 was transfected with expression vectors of CD26 and/or CARMA1. The constructs of Xpress-tagged CARMA1 and its deletion mutant (CARMA1wt, CARMA1 1-742, or CARMA1 1-660, respectively) were made by PCR, using primers described in the Supplementary document. The PCR products were ligated into pcDNA4/HisMax-TOPO (Invitrogen). After constructs were confirmed by DNA sequencing, plasmids were transfected to JPM50.6 cells using Nucleofector II device according to the manufacturer's instruction. Two days after transfection of indicated plasmids, the cells were selected for Blasticidin (1μg/ml, for cells transfected with pEF6/V5 vectors) or Zeocin (10μg/ml, for cells transfected with pcDNA4/HisMax vectors) resistance for 4 weeks. Single clone cells expressing CD26wt (JPM50.6/CD26wt), CARMA1wt (JPM50.6/CARMA1wt), CD26 wt and CARMA1wt (JPM50.6/CD26wt+CARMA1wt), or CD26wt and

CARMA1 (1-660) (JPM50.6/CD26wt+CARMA1 (1-660)) were then selected using standard limiting dilution method.

For stimulation experiments using expression system, CHO-K1 cells were transfected with GFP-fused full length caveolin-1 or SCD-deleted caveolin-1 expression plasmids, with the constructs being described previously (14), using Lipofectamine2000 reagent (Invitrogen). Two days after transfection of indicated plasmids, the cells were selected for G418 (500μg/ml) resistance for 4 weeks. Single clone cells expressing GFP and caveolin-1, detected by anti-caveolin-1 pAb (N20) recognizing the N-terminal region of caveolin-1 using flow cytometry (FCM; FACSCalibur™), were then selected using standard limiting dilution method.

Flow cytometric analysis - For assessment of J.CD26wt that binds biotinylated NT-Fc or NTΔSCD-Fc, 1×10^6 cells were washed in ice-cold PBS, and incubated with Fcγ1 and mouse Ig isotypes (1μg/ml) to block non-specific-binding, followed by reaction with biotynylated NT-Fc, or NTΔSCD-Fc (1μg/ml), and subsequently stained with FITC-conjugated streptavidin (1:500). For blocking experiments, unlabeled mouse IgG (20μg/ml) or unlabeled anti-CD26 mAb (20μg/ml) was incubated with cells prior to reaction with biotynylated NT-Fc or NTΔSCD-Fc. Flow-cytometric analysis of 10,000 viable cells was conducted on FACScalibur™. Each experiment was repeated at least three times, and the results were provided in the form of a histogram or dot plots of a representative experiment.

Small interfering RNA (siRNA) against human CARMA1 - We selected two target sequences from nucleotides +305 to +325 (ss1) and +792 to + 802 (ss2) downstream of the start codon of human CARMA1 mRNA (sense1 siRNA (ss1-siRNA): 5' A AGAGCCCACUCGGAGAUUCUdTdT, and sense2 siRNA (ss2-siRNA): 5' AACUGGAGCGGGAGAAU GAAAdTdT). Moreover, mis-siRNA at 4 nucleotides was prepared to examine non-specific effects of siRNA duplexes (mis-siRNA: 5' UAGUGGCCACAC GGUGATTCdTdT). These selected sequences also were submitted to a BLAST search against the human genome sequence to ensure that only one gene of the human genome was targeted. siRNAs were purchased from QIAGEN. Transfection of siRNA into purified T-cells were conducted using HVJ-E vector (GenomeONE™; kindly provided by IHSIHARA SANGYO KAISHA LTD.) as described previously (14). After 48 hours of transfection, cell were prepared for examination.

T-cell proliferation and IL-2 production assay - For T-cell proliferation assay, 1×10^5 of purified T-cells were cultured in 96-well flat-bottomed plates (COSTAR) in a volume of 200μl of AIM-V medium (GIBCO). For solid-phase stimulation, anti-CD3 (OKT3, 0.05μg/ml) and/or anti-CD26 mAb (5μg/ml), anti-CD28 mAb (4B10, 5μg/ml), or Fc fusion proteins (5μg/ml) were bound on the plates. For stimulation with caveolin-1-transfected CHO cells, purified T-cells were cultured in the presence of soluble anti-CD3 (OKT3, 0.05μg/ml) at 1×10^5 cells/well with varying amounts (T-cells : CHO = 800, 400, 200, 100, 50, 25 : 1, or no CHO cells as background control) of CHO cell transfectants. Before co-culturing with T-cells, CHO transfectants were fixed with 0.05% glutaraldehyde for 30 seconds at room temperature, followed by washing three times with PBS. T-cell proliferation was measured by [^{3}H]-TdR (ICN

Radiochemicals) uptake. Cells were incubated for 96 hours and were pulsed with 1μCi/well of [^{3}H]-TdR, 16 hours prior to harvesting onto a glass-fiber filter (Wallac), and the incorporated radioactivity was quantified by a liquid scintillation counter (Wallac). For blocking experiments, cells were treated with soluble anti-CD26 mAb (1F7), anti-CD28 (4B10), or control mouse Ig (each at 20μg/ml) before being cultured in plates coated with stimulatory-antibodies and/or Fc proteins.

For IL-2 production assay using Jurkat T-cell lines, JPM50.6, or their transfectants, $5x10^5$ cells / well in 200 μl culture media were incubated at 37 °C in the presence of indicated plate-bound antibodies and/or NT-Fc proteins. Cells were also stimulated with PMA (10ng/ml) in anti-CD3-coated wells. After 48 hours of incubation, culture supernatants were pooled from the triplicate wells and assayed for IL-2 content using Human IL-2 Biotrack Easy ELISA (Amersham Biosciences) according to the manufacturer's instruction.

Two-dimensional Polyacrylamide Gel Electrophoresis (2D-PAGE) - For 2D- PAGE analysis of cytosolic proteins, Jurkat cells were lysed in TBSD buffer (50mM Tris-HCl (pH7.6), 150mM NaCl, 2mM EDTA, 0.1% digitonin, 10^2-fold diluted protease inhibitor cocktail, 10^2-fold diluted phosphatase inhibitor cocktail), and then an aliquot (50μg) of lysates was subjected to 2D-PAGE. For pulldown by CD26 AA1-10-Fc, aliquots (1mg) of lysates were precleared by human IgG (2μg) and proteins A-sepharose, followed by immunoprecipitation with Fcγ1 (1μg), or CD26 AA1-10-Fc (1μg). Total lysates or IPs were boiled at 95°C for 3 minutes and supernatants were then resuspended in rehydration lysis buffer (RHB; 8M urea, 2M thiourea, 4%CHAPS, 50mM dithiothreitol, 0.5%ZOOM carrier ampholyte (pH range 3-10) (Invitrogen), 0.002%bromphenol blue). 2D-PAGE and peptide mass mapping were conducted as described previously (15).

Preparation of lysates or lipid raft fractionation, immunoprecipitation and Western blotting - Stimulated or unstimulated cells were pelleted, and lysed with TBSD buffer (50mM Tris-HCl (pH 7.6), 150mM NaCl, 2mM EDTA, 0.1% digitonin, 10^2-fold diluted protease inhibitor cocktail (Sigma), 10^2-fold diluted phosphatase inhibitor cocktail (Sigma)), subjected to immunoprecipitation, followed by SDS-PAGE and Western blot analysis. To obtain the lipid raft fraction, purified T-cells (1×10^8) that were stimulated for 10 minutes with anti-CD3 alone, or with anti-CD3 plus NT-Fc were lysed with 1ml of 1% Triton X-100 and protease inhibitor cocktail in ice-cold MNE buffer (25mM MES (pH6.5) (Sigma), 150mM NaCl, 5mM EDTA), and then fractionated by sucrose gradient centrifugation as described previously (33). For immunoprecipitation of the pooled lipid raft fraction, fractionated lipid rafts were lysed at 4°C for 30 minutes with 1% *N*-octyl-β-D-glucoside (nakarai tesuque), and subjected to immunoprecipitation experiment, followed by SDS-PAGE and Western blot analysis. Immunoprecipitation and Western blot analysis were conducted as described previously (14,15,33).

Nuclear protein extraction and DNA-binding protein assay - Nuclear extracts were prepared from Jurkat cells or transfectats stimulated as indicated, and ELISA-based DNA-binding protein assays for NF-κB p65 were performed using Mercury TransFactor Kits (BD Biosciences) as described previously (14).

Statistics - Student's *t* test was used to determine whether the difference between control and sample was significant ($p < 0.05$ being significant).

RESULTS

We prepared soluble caveolin-1 protein consisting of the putative extracellular N-terminal region or the N-terminal region minus the scaffolding domain (SCD) of human caveolin-1, fused with human IgG_1 Fc (NT-Fc or NTΔSCD-Fc, respectively). The schematic diagrams of the full-length human caveolin-1 protein, NT-Fc, NTΔSCD-Fc and Fcγ1 are shown in Figure 1A. As shown in Figure 1B, while a band of recombinant Fc portion of human IgG_1 (Fcγ1) was observed at *Mr* ~35kDa under reducing conditions (lane 2), the NT-Fc and NTΔSCD-Fc proteins migrated under reducing conditions predominantly as single bands of *Mr* 50kDa and 48kDa, respectively (lanes 3 and 4). Since immunoglobulins are glycosylated posttranslationally, the recombinant Fc fusion proteins produced with mammalian cells had higher *Mr* in SDS-PAGE than as calculated from their amino acid composition(34). In non-reducing conditions, Fcγ1, NT-Fc, or NTΔSCD-Fc were observed at *Mr* ~60kDa, 100kDa, or 90kDa, respectively (lanes 6-8 in Figure 1B), indicating that they were expressed as a homodimer. Fcγ1, NT-Fc, and NTΔSCD-Fc were also evaluated by Western blot analysis using anti-human IgG antibody (Figure 1C).

We examined whether the generated NT-Fc fusion protein binds to CD26. For this purpose, we used Jurkat T-cell line which was stably transfected with full-length human CD26 (J.CD26wt) as described in Experimental Procedures. As shown in Figure 2A, using lysates of J.CD26wt, CD26 was coimmunoprecipitated with NT-Fc (lane 2), but not with Fcγ1 (lane 1) nor NTΔSCD-Fc (lane 3). We next evaluated binding of NT-Fc to cell surface CD26 using FCM. As shown in Figure 2B, cell surface CD26 of J.CD26wt was stained with anti-CD26-FITC mAb ((2) of panel b), while unlabeled CD26 mAb, but not control IgG, blocked staining with anti-CD26-FITC mAb ((3) and (4) of panel b). J.CD26wt was also stained with biotinylated NT-Fc followed by staining with streptavidin-conjugated FITC ((2) of panel c in Figure 2B). Staining with NT-Fc was blocked by unlabeled anti-CD26 mAb ((3) of panel c in Figure 2B) but not control IgG ((4) of panel c in Figure 2B). On the other hand, J.CD26wt was not stained with NTΔSCD-Fc (panel d in Figure 2B). Moreover, native Jurkat T-cells were not stained with anti-CD26 mAb nor with NT-Fc (data not shown). These data suggested that the soluble N-terminal domain of caveolin-1 binds to cell surface CD26, and that the SCD of caveolin-1 is necessary for binding to CD26, as shown in our previous studies (14,15).

To investigate the properties of binding of NT-Fc to CD26, we next examined the binding affinity with the BIAcore system by injecting increasing concentrations of recombinant soluble CD26 (rsCD26) over each sensor surface containing recombinant Fc fusion proteins, Fcγ1, NT-Fc or NTΔSCD-Fc (Figure 2C). rsCD26 did not bind to control recombinant Fcγ1 on a BIAcore sensor chip (panel a in Figure 2C). For each concentration of rsCD26 injected, the binding response at equilibrium was calculated by subtracting the response observed in

NT-Fc, resulting in a K_d value of ~2×10^{-5} M by equilibrium binding analysis (panel b in Figure 2C). rsCD26 did not bind to NTΔSCD-Fc on a BIAcore sensor chip (panel c in Figure 2C). These results clearly indicated that the N-terminal domain of caveolin-1 binds directly to CD26.

We next evaluated whether NT-Fc stimulation had similar effect as anti-CD26 mAb on CD26-mediated T-cell costimulation in J.CD26wt (13). As shown in Figure 2D, IL-2 production of J.CD26wt induced by plate-bound anti-CD3 plus NT-Fc was observed to be at a similar level as that induced by anti-CD3 plus anti-CD28 or by anti-CD3 plus anti-CD26 (*,** and *** in the bar graph), while IL-2 production was not observed in JKTwt (which is CD26 negative) following stimulation by anti-CD3 plus anti-CD26 nor by anti-CD3 plus NT-Fc (* and *** in Figure 2D). IL-2 production by J.CD26wt or JKTwt was not observed with the use of control recombinant Fcγ1 nor NTΔSCD-Fc (# in Figure 2D). To further investigate whether the T-cell costimulatory activity of NT-Fc was exerted via CD26, blocking experiments were conducted using CD26-specific mAb which blocked binding of NT-Fc to J.CD26wt. As shown in Figure 2E, IL-2 production induced by plate-bound anti-CD3 plus anti-CD26 was blocked by soluble anti-CD26 mAb, but not by soluble anti-CD28 mAb (** and ##). In this experimental condition, IL-2 production induced by plate-bound anti-CD3 plus NT-Fc was blocked by soluble anti-CD26 mAb, but not by soluble anti-CD28 mAb (* and # in Figure 2E). Control Fγc1 or NTΔSCD-Fc did not have any T-cell costimulatory activity (Figure 2E). Taken together, our results clearly indicated that caveolin-1 binds directly to CD26, and induces T-cell costimulation via CD26.

We next evaluated the ability of NT-Fc to reproduce the effects of anti-CD26 mAb on CD26-mediated T-cell costimulation (11,35). As shown in Figure 3A, T-cell proliferation induced by plate-bound anti-CD3 plus NT-Fc was observed to be at a similar level as that induced by anti-CD3 plus anti-CD28 or by anti-CD3 plus anti-CD26 (* in the bar graph), while T-cell proliferation was not observed using control recombinant Fcγ1 nor NTΔSCD-Fc (** in the bar graph). Moreover, T-cell costimulation induced by NT-Fc was observed in a dose-dependent manner, while increasing doses of Fcγ1 or NTΔSCD-Fc did not induce T-cell proliferation (Figure 3B). To further define the costimulatory activity of caveolin-1, we prepared CHO cells stably expressing human caveolin-1. As shown in Figure 3C, we then showed that Cav-wt^+ CHO cells expressed T-cell costimulatory activity in the presence of anti-CD3 mAb, an effect not observed with $mock^+$ CHO cells nor Cav-ΔSCD^+ CHO cells. The costimulatory activity of Cav-wt^+ CHO cells was further observed in a cell number-dependent manner (* in Figure 3C).

To further investigate whether the T-cell costimulatory activity of NT-Fc is exerted via CD26, blocking experiments were conducted using CD26-specific mAb which blocked binding of NT-Fc to J.CD26 (Figures 2B). As shown in Figure 3D, T-cell proliferation by plate-bound anti-CD3 plus anti-CD26 was blocked by soluble anti-CD26 mAb, but not by soluble anti-CD28 mAb (*). On the other hand, T-cell proliferation by plate-bound anti-CD3 plus anti-CD28 was blocked by soluble anti-CD28 mAb, but not by soluble anti-CD26 mAb (** in Figure

3D). In this experimental condition, T-cell proliferation by plate-bound anti-CD3 plus NT-Fc was blocked by soluble anti-CD26 mAb, but not by soluble anti-CD28 mAb (*** in Figure 3D). Control Fγc1 or NTΔSCD-Fc did not have any T-cell costimulatory activity (Figure 3D). Moreover, blocking effect of CD26-specific mAb on NT-Fc costimulation was observed in a dose-dependent manner (* in Figure 3E), and control IgG or anti-CD28 mAb at concentrations of 0-50μg/ml did not block NT-Fc costimulation (Figure 3E). Taken together with data shown in Figures 1-3, these data suggested that NT-Fc functionally engages CD26 and not nonspecific proteins, and that caveolin-1 has a costimulatory effect on T-cell proliferation via the TCR/CD3 pathway.

The proximal signaling molecules of CD26-mediated T-cell costimulation by caveolin-1 were next determined. We first examined whether the cytoplasmic tail of CD26 is responsible for T-cell costimulation by NT-Fc in the presence of anti-CD3 mAb. For this purpose, costimulation experiments were performed on Jurkat T-cells transfected with CD26-CD10 chimeric receptor. Moreover, while CD26 is reported to form homodimers on cell surface (36,37), it remains to be determined whether dimeric CD26 is responsible for CD26-mediated T-cell costimulation. Therefore, costimulation experiments were conducted using Jurkat T-cells transfected with monomeric CD26 (CD26 H750E). We first verified the Jurkat stable transfectants; as shown in Figure 4A, while CD26wt, CD26+CD10 cyto and CD26 H750E were detected at *Mr* ~100kDa in reducing conditions (lanes 2-4), bands of CD26wt and CD26+CD10 cyto migrated at *Mr* ~200kDa (lanes 6 and 7) and a band of CD26 H750E migrated at *Mr* 100 kDa (lane 8) in non-reducing conditions, indicating that CD26wt and CD26+CD10 cyto exist as dimers and CD26 H750E exists as monomers in the Jurkat transfectants. Moreover, as shown in Figure 4B, by immunoprecipitation using anti-V5 mAb, V5-tagged CD26 was detected by anti-CD26 mAb in each of transfectant (CD26wt, CD26+CD10 cyto, or CD26 H750E) in reducing SDS-PAGE (lanes 2-4). Furthermore, Figure 4C showed the cell surface expression of CD3 and CD26 in Jurkat transfectants. CD3 was expressed at similar intensity among transfectants (horizontal axis of panels a-d in Figure 4C), while the intensity of cell surface CD26 expression was different between CD26wt/CD26+CD10 cyto and CD26 H750E (vertical axis of panels b-d in Figure 4C), suggesting a difference between dimeric expression and monomeric expression. CD26 was not observed in mock-vector transfected Jurkat (JKT/mock) (panel a in Figure 4C). Using these Jurkat transfectants, costimulation experiments by NT-Fc were conducted. As shown in Figure 4D, IL-2 production was observed in CD26wt transfected Jurkat T-cells by stimulation with anti-CD3 plus NT-Fc (* in panel a), but not in CD26-CD10 chimera nor in CD26 H750E transfected Jurkat. Moreover, p65, one of NF-κB components, was activated in CD26wt transfected Jurkat T-cells following stimulation with anti-CD3 plus NT-Fc (* in panel b), but not in CD26-CD10 chimera nor in CD26 H750E transfected Jurkat. Furthermore, IL-2 production or p65 induction by stimulation with anti-CD3 plus PMA was equally observed in either of CD26wt, CD26-CD10 chimera, or CD26 H750E transfected Jurkat (panels a and b of Figure 4D).

These data strongly suggested that the cytoplasmic tail of dimeric CD26, but not of monomeric CD26, is responsible for T-cell costimulation by NT-Fc in the presence of anti-CD3 mAb.

Since the cytoplasmic tail of CD26 appears to play a key role for CD26-mediated T-cell costimulation as shown in Figure 4, we next explored signaling molecules associated with the cytoplasmic tail of dimeric CD26. For this purpose, we prepared Fc fusion protein containing the first 10-aa of the N-terminal residues of CD26 (CD26 AA1-10-Fc) (Figures 5A). As shown in Figure 5B, purified protein of CD26 AA1-10-Fc was observed at *Mr* ~37kDa in reducing conditions (lane 3), and at *Mr* ~70kDa in non-reducing conditions (lane 6), suggesting that CD26 AA1-10-Fc formed homodimers. Following pulldown by CD26 AA1-10-Fc of Jurkat T-cell lysates, molecules that interacted with CD26 AA1-10-Fc were analyzed by 2D SDS-PAGE. The gel of 2-D PAGE using input lysates is shown in Figure 5C (panel a). Compared to 2-D gel analyzing IP complex by control Fcγ1 (panel b in Figure 5C), six spots were detected by pulldown assays with CD26 AA1-10-Fc (panel c in Figure 5C). Using MALDI-TOF MS the proteins were determined to be (spot #1) epidermal cytokeratin 2 (*Mr* ~66kDa), (spot #2) glutamyl-tRNA synthetase (*Mr* ~70kDa), (spot #3) tubulin (*Mr* ~50kDa), (spot #4) Unnamed protein (*Mr* ~84kDa), (spot #5) CARMA1 (*Mr* ~120kDa), or (spot #6) HSP70 (*Mr* ~55kDa), respectively (panel c in Figure 5C). Following five independent repeats of these experiments with similar results, the unnamed protein (spot #4) was not identified more precisely by this procedure, and the other spots other than CARMA1 were ubiquitously expressed as housekeeping proteins. Therefore, CARMA1 was identified as an interacting protein with the cytoplasmic tail of CD26, and subjected to further examination.

For further confirmation, we next performed immunoprecipitation (IP) studies using lysates of J.CD26wt. As shown in Figure 5D, CD26 was detected in a complex of lysates coprecipitated with anti-CARMA1 pAb (lane 2 of upper panel), while not coprecipitated with control goat IgG (lane 1 of upper panel). Moreover, CARMA1 was detected in a complex of lysates coprecipitated with anti-CD26 mAb (lane 4 of lower panel in Figure 5D), while not coprecipitated with control mouse IgG (lane 3 of lower panel in Figure 5D). These data suggested that CARMA1 binds to CD26 in cells. To determine the binding domain between CD26 and CARMA1, coimmunoprecipitation assay was next performed using 293FT-cells cotransfected with Xpress-tagged human full-length CARMA1 (CARMA1wt) and with CD26wt, CD26+CD10 cyto, or CD26 H750E. As shown in Figure 5E, CARMA1 was coprecipitated with CD26wt (lane 2), but not with CD26+CD10 cyto, nor CD26 H750E (lanes 3 and 4). These data strongly suggested that the cytoplasmic tail and dimerization of CD26 are necessary to interact with CARMA1. We next explored the binding domain of CARMA1 to CD26. For this purpose, we prepared the C-terminal truncated deletion mutants of CARMA1 (Figure 5F). As shown in Figure 5G, CD26 was coprecipitated with CARMA1wt or with CARMA1 1-742 (lanes 2 and 3), but not with CARMA1 1-600 (lane 4), suggesting that the PDZ domain in CARMA1 was necessary for binding to CD26.

To explore the role of CARMA1 in CD26-mediated T-cell costimulation, we used

CARMA1-deficient Jurkat T-cell lines JPM50.6 to conduct rescue experiments (18). As shown in Figure 6A, CARMA1 and CD26 was not detected in JPM50.6 (lane 3 of upper and lower panels), while CARMA1 was expressed in native Jurkat and J.CD26wt (lanes 1 and 2 of lower panel), and CD26 was expressed in J.CD26wt (lane 2 of upper panel), but not in native Jurkat (lane 1 of upper panel). We next generated the stable transfectants using JPM50.6 as described in Experimental Procedures. Figure 6B shows that transfected Xpress-tagged CARMA1 was expressed in JPM50.6/CARMA1wt, JPM50.6/CD26wt+CARMA1wt and JPM50.6/CD26wt+CARMA1 (1-660), and that transfected V5-tagged CD26 was expressed in JPM50.6/CD26wt, JPM50.6/CD26wt+CARMA1wt and JPM50.6/CD26wt+CARMA1 (1-660). Figure 6C shows the cell surface expression of CD3 and CD26 in JPM50.6 transfectants. CD3 was expressed at similar intensity among transfectants (horizontal axis of panels a-e in Figure 6C). While the intensity of cell surface CD26 expression was similar among JPM50.6/CD26wt, JPM50.6/CD26wt+CARMA1wt and JPM50.6/CD26wt+CARMA1 (1-660) (panels b, d, and e in Figure 6C), CD26 was not observed in JPM50.6/V (mock vector) and JPM50.6/CARMA1wt (panels a and c in Figure 6C). Using these transfectants, IL-2 production and NF-κB activation assays were performed with stimulation by anti-CD3 alone or anti-CD3 plus NT-Fc. As shown in Figure 6D, IL-2 production induced by anti-CD3 plus NT-Fc was clearly observed in JPM50.6/CD26wt+CARMA1, but not in JPM50.6, JPM50.6/CD26wt, JPM50.6/CARMA1, or JPM50.6/CD26wt+CARMA1 (1-660) (panel a). Similarly, NF-κB activation induced by anti-CD3 plus NT-Fc was clearly observed in JPM50.6/CD26wt+CARMA1, but not in JPM50.6, JPM50.6/CD26wt, JPM50.6/CARMA1, or JPM50.6/CD26wt+CARMA1 (1-660) (panel b in Figure 6D). Furthermore, IL-2 production or NF-κB activation by stimulation with anti-CD3 plus PMA was equally observed in either of transfectants (panels a and b of Figure 6D). Taken together, these results suggested that CARMA1 is necessary to exert CD26-mediated costimulation by NT-Fc.

As shown above, costimulation of CD26 is observed to be exerted via interaction of CD26 with CARMA1 in the cytoplasm in Jurkat cells. To confirm this interaction more profoundly, we performed biochemical assays using human T-cells purified from healthy adult peripheral blood mononuclear cells (APB-T-cells). For this purpose, we first conducted immunoprecipitation (IP) studies using lysates of APB-T-cells. As shown in Figure 7A, CD26 was detected in a complex of lysates coprecipitated with anti-CARMA1 pAb (lane 2 of upper panel), while not coprecipitated with control goat IgG (lane 1 of upper panel). Moreover, CARMA1 was detected in a complex of lysates coprecipitated with anti-CD26 mAb (lane 4 of lower panel in Figure 7A), while not coprecipitated with control mouse IgG (lane 3 of lower panel in Figure 7A). These data suggested that CARMA1 binds to CD26 in normal T-cells.

We previously showed that non-activated peripheral blood T-cells treated with the anti-CD26 mAb 1F7 resulted in CD26 recruitment to lipid rafts, concomitant with increased tyrosine phosphorylation of ZAP70, $p56^{lck}$, and TCRζ (33). Other investigators have reported that, in the process of

activation of NF-κB via CD3 costimulation, CARMA1 was recruited to lipid rafts along with Bcl10, and IKKβ (18,25,27,38,39). We hence examined whether CD26 and CARMA1 are recruited to lipid rafts by anti-CD3 plus caveolin-1 costimulation in normal T-cells. For this purpose, using a sucrose-gradient separation method, we prepared lipid raft fractions of APB-T-cell lysates in the presence or absence of anti-CD3 plus NT-Fc costimulation. As shown in Figure 7B, following stimulation with anti-CD3 plus NT-Fc, CD26, CARMA1, Bcl10, and IKKβ were detected in the lipid raft fractions, while CD26, CARMA1, Bcl10, and IKKβ were not detected in the lipid raft fractions after stimulation with anti-CD3 alone. Moreover, time-course analysis revealed that CD26, CARMA1, Bcl10, and IKKβ were migrated into lipid rafts after stimulation with anti-CD3 plus NT-Fc (Figure 7C), while CD26, CARMA1, Bcl10, and IKKβ were not detected after anti-CD3 treatment (data not shown). Furthermore, to examine whether CD26 and CARMA1 forms a complex with Bcl10 and IKKβ in lipid rafts, coprecipitation assay was performed using lipid raft fractions of APB-T-cell lysates from cells costimulated with anti-CD3 plus NT-Fc. As shown in Figure 7D, CD26, CARMA1, Bcl10, and IKKβ in lipid rafts were coprecipitated with CD26 (lane 4), while not detected in the lysates of APB-T-cells following stimulation with anti-CD3 alone (lane 2). Taken together, these data indicated that ligation of CD26 by caveolin-1 recruits a complex of CARMA1, Bcl10, and IKKβ to lipid rafts in normal T-cells.

To examine the role of CARMA1 on CD26-mediated T-cell costimulation more directly, we performed siRNA experiments in freshly isolated APB-T-cells. For this purpose, we prepared 2 sets of specific siRNA against CARMA1 as described in Experimental Procedures, and both of these siRNA decreased CARMA1 expression in APB-T-cells, while the expression levels of CD26, TCR-β or β-actin were not changed in the presence of control siRNA, ss1-siRNA, or ss2-siRNA (inside box of Figure 7E). After transfection of these siRNAs into APB-T-cells, proliferation assay was performed in the presence of anti-CD3 plus NT-Fc stimulation. As shown in Figure 7E, T-cell proliferation stimulated with anti-CD3 plus NT-Fc was decreased in T-cells treated with siRNAs against CARMA1 while T-cell proliferation was observed in T-cells treated with control siRNA (* in Figure 7E). Moreover, T-cell proliferation stimulated with anti-CD3 plus PMA was observed in either of control siRNA, ss1 or ss2-siRNA (** in Figure 7E). These results suggested that CARMA1 plays an important role in signal transduction following CD26 binding to caveolin-1, leading to T-cell proliferation in normal T-cells.

DISCUSSION

In this study, we showed that caveolin-1 is the costimulatory ligand for CD26, and that ligation of CD26 by caveolin-1 induces T-cell proliferation and NF-κB activation with costimulation of TCR/CD3. Moreover, we showed that the cytoplasmic tail of CD26 in T-cell interacts with CARMA1, resulting in signal transduction leading to NF-κB activation, and that ligation of CD26 by caveolin-1 recruits a complex of CD26, CARMA1, Bcl10, and IKKβ to lipid rafts.

Enhancement of CD26 expression in autoimmune diseases may correlate with disease

severity (40,41), since patients with autoimmune diseases such as Grave's disease and rheumatoid arthritis have increased levels of CD26+T-cells in their peripheral blood as well as inflamed tissues, including thyroid and synovial fluids and membranes (9,42). These findings imply that CD26+T-cells play a role in the inflammation process and subsequent tissue destruction. Originally characterized as a T-cell activation antigen, human CD26 is preferentially expressed on the CD4+ memory T-cell subset, and is upregulated after T-cell activation (2,3,10). Along with its enhanced expression on activated T-cells, various lines of evidence have converged to demonstrate that CD26 is functionally associated with T-cell signal transduction processes relating to T-cell activation (2,10,11,43). However, the precise mechanism involved in T-cell activation via CD26 in response to memory antigen such as tetanus toxoid remains to be clearly characterized, including the identification of its costimulatory ligand and the associated proximal signaling molecules. Recently, we demonstrated that CD26 binds to caveolin-1 on APC, and that residues 201 to 211 of CD26 along with the serine catalytic site at residue 630, which constitute a pocket structure of CD26/DPPIV, contribute to binding to the caveolin-1 scaffolding domain (14). This region in CD26 contains a caveolin-binding domain (CBD) ($\Phi X\Phi XXXX\Phi XX\Phi$; Φ and X depict aromatic residue and any amino acid, respectively), specifically WVYEEEVFSAY in CD26 (2,44). These observations strongly support the notion that DPPIV enzyme activity is necessary to exert T-cell costimulatory activation via CD26 as demonstrated in our previous report using CD26 specific mAbs (13).

To examine the binding of caveolin-1 to CD26 in T-cells, we used soluble Fc fusion proteins containing the N-terminal domain of caveolin-1 (NT-Fc) (Figure 1), and found that NT-Fc binds specifically to CD26 to induce T-cell proliferation in the presence of TCR/CD3 costimulation (Figures 2 and 3). Moreover, the binding affinity between caveolin-1 and CD26 ($K_d \sim 2\times10^{-5}$ M) as determined by the BIAcore system (Figure 2C) is comparable to that of other costimulatory molecules with important roles in immune responses and their associated ligands, such as CD2-CD5 ($K_d \sim 10^{-6}$ M), CD80-CD28 ($K_d \sim 10^{-7}$ M) and CD86-CD28 ($K_d \sim 10^{-6}$ M) (45-47). Until now, CD26-mediated T-cell costimulation was performed using anti-CD26 mAbs, resulting in various CD26 functions (4,7,48,49). Assuming that the affinity between antigen and antibody is higher ($K_d \sim 10^{-9}$ M) than that of a ligand-receptor system, and that ligand-specific conformations are capable of differentially activating distinct signaling partners (50), ligand-dependent pathways may be predicted to have different signals associated with the antigen-antibody system and ligand-receptor system.

We have demonstrated previously that ligation of CD26 by the anti-CD26 mAb 1F7 induces T-cell costimulation and IL-2 production by CD26-transfected Jurkat T-cell lines, while increasing tyrosine phosphorylation of signaling molecules such as ZAP70, $p56^{lck}$ and CD3ζ was observed (2,7,12). In addition, we have shown that ligation of the CD26 molecules by the anti-CD26 mAb 1F7 increases the recruitment of CD26 molecules with CD45RO to lipid rafts, resulting in increased tyrosine phosphorylation of signaling molecules (33). However, the precise proximal signaling pathway of CD26 has not yet been